Applied Acoustics xxx (xxxx) xxx–xxx

Contents lists available at ScienceDirect

Applied Acoustics

journal homepage: www.elsevier.com/locate/apacoust

A study on helicopter main gearbox planetary bearing fault diagnosis

Linghao Zhou[a,*], Fang Duan[a], Michael Corsar[b], Faris Elasha[c], David Mba[d]

[a] School of Engineering, London South Bank University, London, UK
[b] CSAIC, and Centre for Propulsion, Cranfield University, Milton Keynes, UK
[c] School of Mechanical, Automotive and Aerospace Engineering, Coventry University, UK
[d] Faculty of Technology, De Montfort University, Leicester, UK

ARTICLE INFO

Keywords:
Helicopter main gearbox
Planetary bearing
Self-adaptive noise cancellation
Kurtogram
Envelope analysis
Condition monitoring

ABSTRACT

The condition monitoring of helicopter main gearbox (MGB) is crucial for operation safety, flight airworthiness and maintenance scheduling. Currently, the helicopter health and usage monitoring system, HUMS, is installed on helicopters to monitor the health state of their transmission systems and predict remaining useful life of key helicopter components. However, recent helicopter accidents related to MGB failures indicate that HUMS is not sensitive and accurate enough to diagnose MGB planetary bearing defects. To contribute in improving the diagnostic capability of HUMS, diagnosis of a MGB planetary bearing with seeded defect was investigated in this study. A commercial SA330 MGB was adopted for the seeded defect tests. Two test cases are demonstrated in this paper: the MGB at 16,000 rpm input speed with 180 kW load and at 23,000 rpm input speed with 1760 kW load. Vibration data was recorded, and processed using signal processing techniques including self-adaptive noise cancellation (SANC), kurtogram and envelope analysis. Processing results indicate that the seeded planetary bearing defect was successfully detected in both test cases.

1. Introduction

Helicopters have been extensively employed for various civil and industrial purposes in modern society. Their versatilities come from the capabilities of performing unique manoeuvres including direct take-off, landing and hovering to fulfil special needs during operations. A well-functioned main gearbox (MGB) contributes critically to a helicopter's airworthiness, i.e. the suitability for safety flight, because that MGB takes vitally important responsibilities to reduce high input speed generated from engines, providing appropriate torque to main rotors and other accessory systems. The working principle of MGB system determines that the friction heat and excessive mechanical forces applied to MGB key components are significant. MGB key components including shafts, planetary gears and bearings suffer from such harsh operational conditions, and are vulnerable to fatigue defects. Therefore, health and usage monitoring system (HUMS) is developed to monitor the health condition of MGB as well as other helicopter's key components, aiming to enhance the helicopters' operational reliability and functionality, support maintenance decision making, improve flight airworthiness and reduce overall maintenance costs.

The investigation of employing HUMS as the condition monitoring system for helicopters was initiated in 1982 [1]. In 1990, the United Kingdom Civil Aviation Authority (UK CAA) made it mandatory to install Flight Data Recording (FDR) unit on medium and large civil helicopters to monitor their flight status. To this day, HUMS developed by companies and organisations including Airbus, GE Aviation, Goodrich, and Honeywell among many others are in service [2].

Generally, HUMS conducts helicopter health monitoring by recording vibration data to produce condition indicators (CIs). Anomalies of online CIs caused by defects will trigger the system alarms so that pilots can react accordingly. In-depth post-analysis is performed at ground station, where all CIs are checked for fault-related overflow, so that maintenances can be scheduled proactively. The implementation of HUMS has contributed to reducing helicopter accident rate without doubts. According to a survey conducted by International Helicopter Safety Team (IHST) on worldwide helicopter accident rate, it is evident that the accident rate has dropped from 9.4 accidents per 100,000 flight hours to approximately 6.5 accidents per 100,000 flight hours, from year 2005 to 2011 [3]. Nevertheless, it is concerning that the HUMS does not perform reliably and effectively in detecting MGB planetary bearing defects [4]. For example, official investigation for G-REDL accident carried out by Air Accidents Investigation Branch (AAIB) suggested that, root cause for this accident was planetary gear fracture, which was originated from the planetary bearing outer race [5]. G-REDW accident happened in 2012 was caused by MGB lubrication system and emergency lubrication system failure, due to MGB vertical

* Corresponding author.
E-mail address: zhoul7@lsbu.ac.uk (L. Zhou).

https://doi.org/10.1016/j.apacoust.2017.12.004
Received 7 July 2017; Received in revised form 7 December 2017; Accepted 8 December 2017

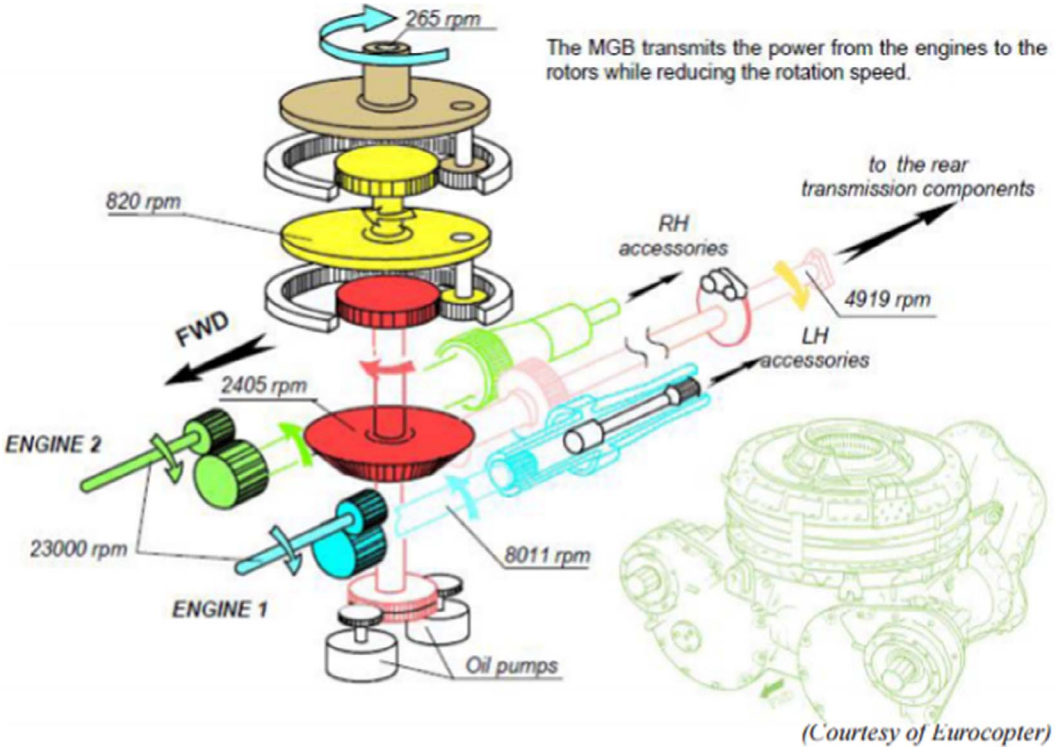

Fig. 1. MGB internal configuration [5].

Table 1
MGB speed reduction ratios.

Maximum input speed	23,000 rpm
Maximum output speed	265 rpm
Input shaft reduction ratio	1:2.87
Intermediate shaft reduction ratio	1:1.63
Bevel stage reduction ratio	1:2.05
1st Epicyclic module Ratio	1:3.10
2nd Epicyclic module Ratio	1:2.91

Table 2
Number of planetary bearings and their corresponding rollers.

	Planetary bearings	Number of rollers
1st Epicyclic module	8	17
2nd Epicyclic module	9	13

bevel gear crack [6]. In 2016, helicopter LN-OJF crashed in Norway, post-analysis suggested this accident was resulted from fatigue fracture in one of the eight second stage planetary bearings, with clear similarities to the G-REDL accident [7]. In these and many other helicopter accidents where people were severely injured or even lost their lives, HUMS and CIs have failed to generate accurate warnings against MGB planetary bearing related defects. Therefore, successful diagnosis of planetary bearing defect in MGB could contribute profoundly to enhancing sensitivity of HUMS against such defect type, and improving helicopter flight safety.

Over the last two decades, significant research has been undertaken in the study of bearing fault diagnosis. In [8,9], Ho and Randall implemented self-adaptive noise cancellation (SANC) technique to separate deterministic gear mesh signals and non-deterministic bearing signals. Such technique was further evaluated extensively in [10–12]. Envelope analysis has been established as a benchmark technique to extract the diagnostic information hidden in high frequency resonances [13–15]. Antoni and Randall developed kurtogram based on the concept of spectral kurtosis (SK), and proposed using kurtogram as a frequency resonance detector in conjunction with envelope analysis [16]. Implementing the aforementioned techniques has undoubtedly

(a) 2^{nd} Planetary gears/ bearings

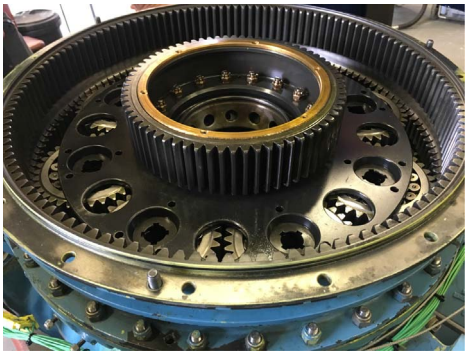

(b) 2^{nd} Epicyclic module ring and sun gears

Fig. 2. MGB 2nd epicyclic module.

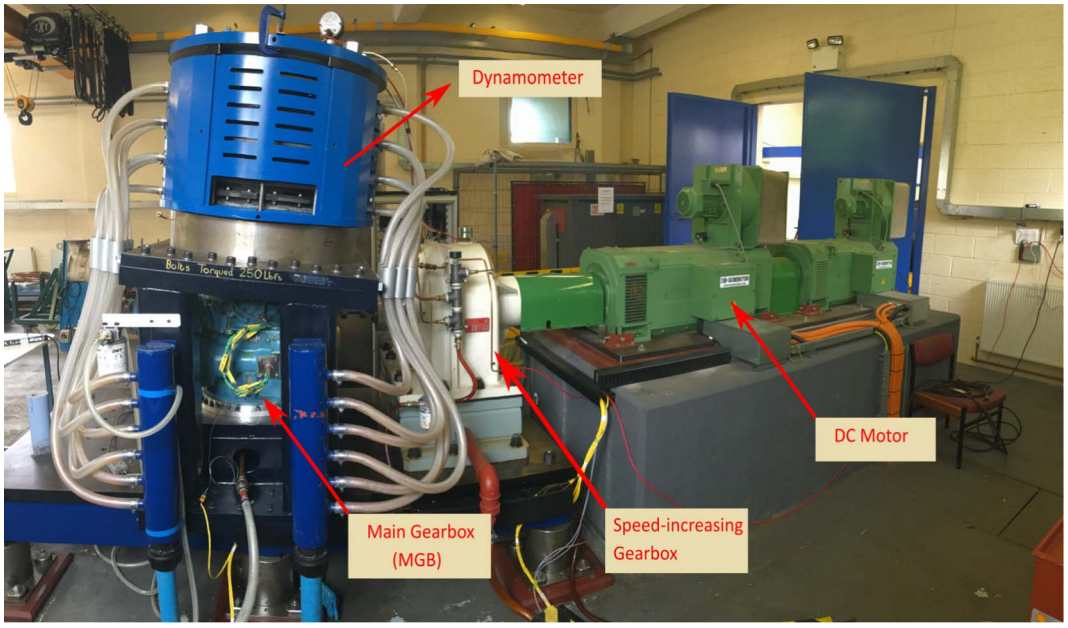

Fig. 3. Demonstration of MGB test rig.

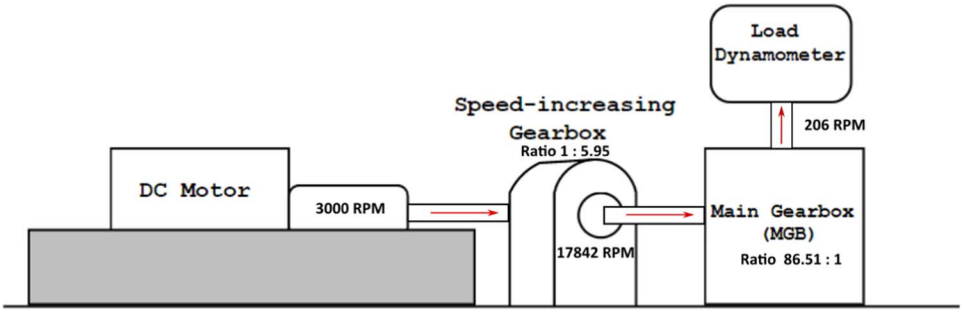

Fig. 4. Schematic diagram of the test rig.

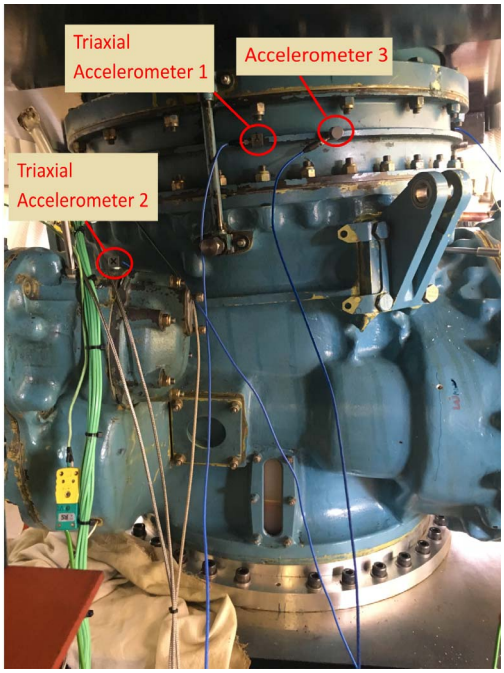

(a) Sensor installation side view

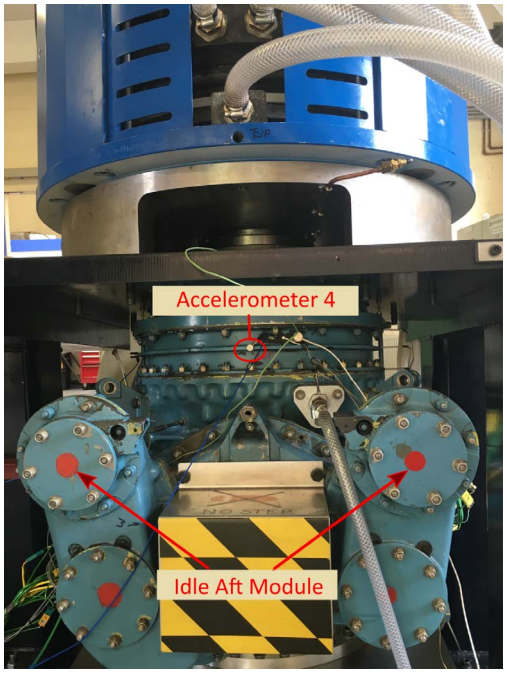

(b) Sensor installation front view

Fig. 5. Demonstration of accelerometers installation locations.

Table 3
Installation locations of accelerometers.

Sensor no.	Sensor type	Location
1	Triaxial	Middle of 1st and 2nd epicyclic case
2	Triaxial	High speed input module
3	Uniaxial	Middle of 1st and 2nd epicyclic case
4	Uniaxial	Middle of 1st and 2nd epicyclic case

Fig. 6. The components of 2nd planetary bearing.

Table 4
Dimensions of seeded bearing defects.

	Length (mm)	Width (mm)	Depth (mm)
Minor defect	5	3	1.5
Major defect	8	6	2.5

(a) Minor Defect

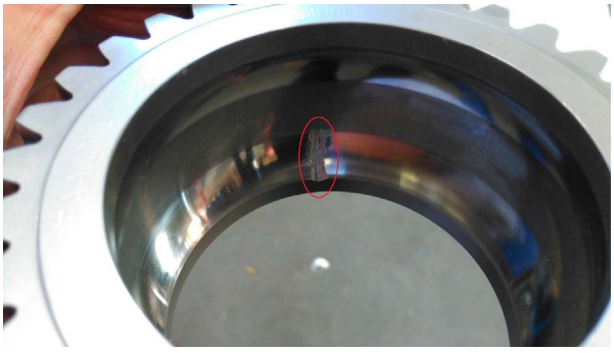

(b) Major Defect

Fig. 7. Demonstration of seeded defects in test case 1.

achieved successes on diagnosing bearing fault, but most of these investigations were carried out on simulated data or experimental data taken from bearings in a relatively simplified system or test-rig. An actual operational helicopter MGB is a very sophisticated mechanical system, containing multiple speed reduction modules and planetary stages. Therefore, vibration data collected from helicopter MGB reflects complex mechanics of interactions between gears and bearings in MGB that can hardly be simulated. Diagnosis of planetary bearing defects in an operating MGB is considered to be more challenging in this regard.

To investigate planetary bearing defect diagnosis, valuable experimental vibration data was acquired from a helicopter MGB operated under two test cases, with emphasis on different test conditions in terms of defect sizes, operating speed and load.

2. Experimental rig and setup

2.1. Introduction on the main gearbox

A *Category A* Super Puma SA330 MGB was adopted for the experimental tests. In Fig. 1, the internal configuration of MGB is illustrated. The MGB has an input speed specification of approximately 23,000 rpm. The input speed from the engines is reduced via several gear reduction stages, reduction ratios are listed in Table 1.

To investigate planetary bearing fault diagnosis, defects were seeded on the outer race of the planetary bearing at 2nd epicyclic module in both test cases. Fig. 2(a) demonstrates 2nd epicyclic planetary bearings, which are driven by 2nd epicyclic sun gear and ring gear shown in Fig. 2b. Specifications of planetary bearings are documented in Table 2.

2.2. Test case 1

2.2.1. Experimental rig

Fig. 3 demonstrates the test rig designed for test case 1. The test rig consisted of a SA330 MGB, a speed-increasing gearbox, a DC motor and a dynamometer. The schematic diagram of the test rig is shown in Fig. 4. The DC motor is able to generate 3000 rpm speed. The speed-increasing gearbox connected with DC motor can significantly boost the speed up to 17,842 rpm to drive one of the MGB's input shaft. The absorption dynamometer was installed on top of the 2nd epicyclic module, creating desired loading for MGB.

2.2.2. Sensor selection and installation

In this test case, 2 triaxial and 2 uniaxial accelerometers were installed to capture MGB's vibration information. Originally, accelerometers with 100 mV/g high measuring sensitivity and 50 g measuring range were selected. However, preliminary test results showed that the amplitude of recorded vibration can reach approximately 500 g, which saturated the high sensitivity accelerometers. Therefore, uniaxial accelerometers PCB 352C03 and triaxial accelerometers PCB 356A43 were selected, which have 10 mV/g sensitivity and 500 g measuring range. All accelerometers were mounted at the MGB case externally.

The rules of placing sensors are platform/mission specific [17]. Generally, sensors should be installed as close as practical to the components they are intended to monitor, while not affecting mechanical structures of the components [18]. Fig. 5 shows the installation locations of the accelerometers. Two triaxial accelerometers were allocated to monitor epicyclic modules and input shaft (accelerometer 1 and 2, respectively). Other two uniaxial accelerometers were installed in the middle of the two epicyclic modules to provide comparative information. Table 3 describes above installation arrangements.

2.2.3. Test procedures

This test case was focused on detecting planetary bearing defects in their incipient stage, i.e. defects are localised. To insert incipient defects

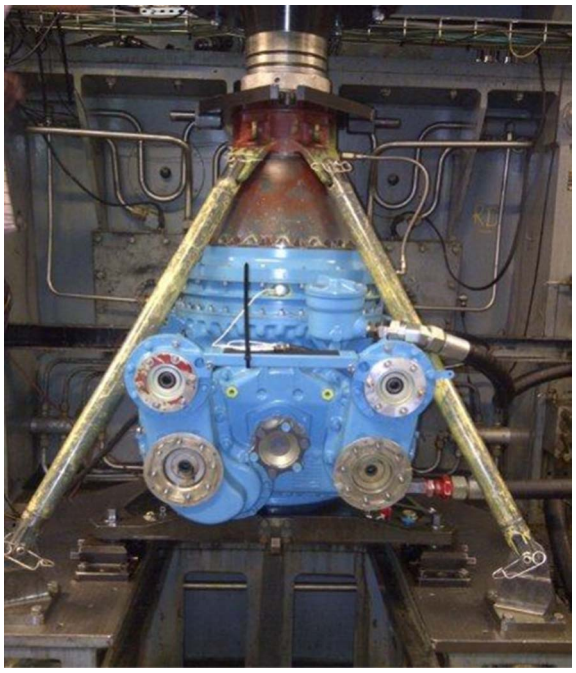

Fig. 8. MGB mounted on the test bench in test case 2 [19].

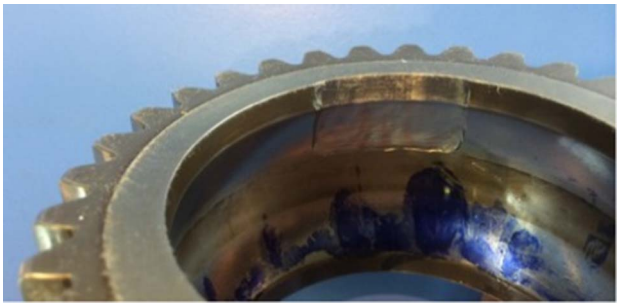

Fig. 9. A demonstration of seeded major bearing defect in test case 2 [19].

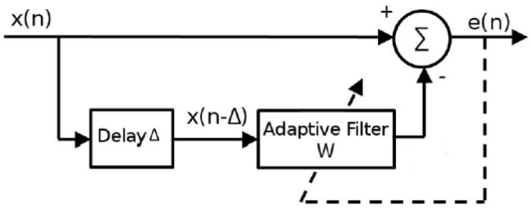

Fig. 10. Schematic diagram of SANC [10].

Table 5
Key frequency components of test case 1.

Speed of:	Frequency [Hz]
Input shaft	266.67
1st planetary carrier shaft	9.01
1st planetary gear meshes	1171.09
2nd planetary carrier shaft	3.09
2nd planetary gear meshes	402.19
Outer race defect frequency (f_{ORD}):	67.77

on the outer race of 2nd epicyclic planetary bearing, a 2nd epicyclic planetary bearing was disassembled (Fig. 6). The bearing had two layers of races, as well as two sets of rollers and cages.

The test procedures consisted of three test conditions, including healthy condition, minor seeded defect condition and major seeded defect condition. The dimensions of seeded defects are detailed in Table 4. Pictures of minor and major defects are presented in Fig. 7. As introduced in Section 2.2.1, the maximum speed from speed-increasing gearbox to MGB was limited to 17,842 rpm. To comply with safety protocols, the maximum load and input speed in all test conditions were limited to 180 kW and 16,000 rpm respectively. Between each test, the MGB was stripped for 3 days to allow swapping the faulty bearing. Vibration data was recorded using NI 9234 data acquisition card and sampled at 25.6 kHz frequency.

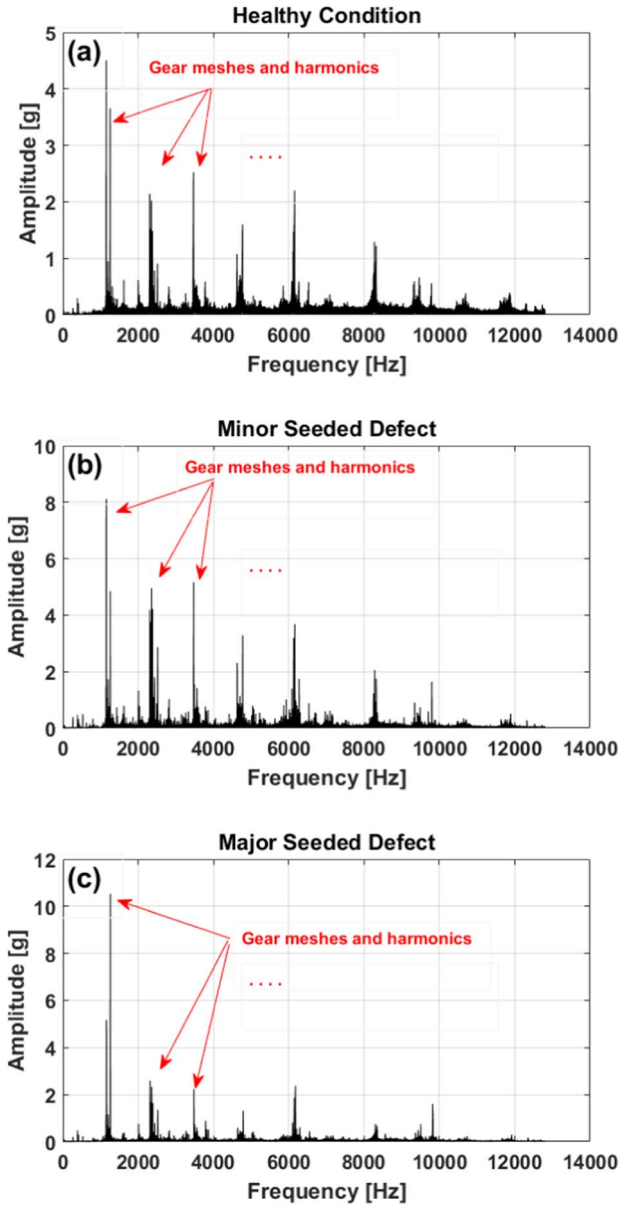

Fig. 11. Amplitude spectrum of raw data in (a) healthy condition, (b) minor seeded defect condition and (c) major seeded defect condition.

2.3. Test case 2

2.3.1. Experimental rig

In this test case, an identical SA330 MGB was installed at special test bench which enabled both input shafts to be operated. This test bench is different from the experimental rig described in Test case 1. Fig. 8 demonstrates the MGB mounted on the test bench.

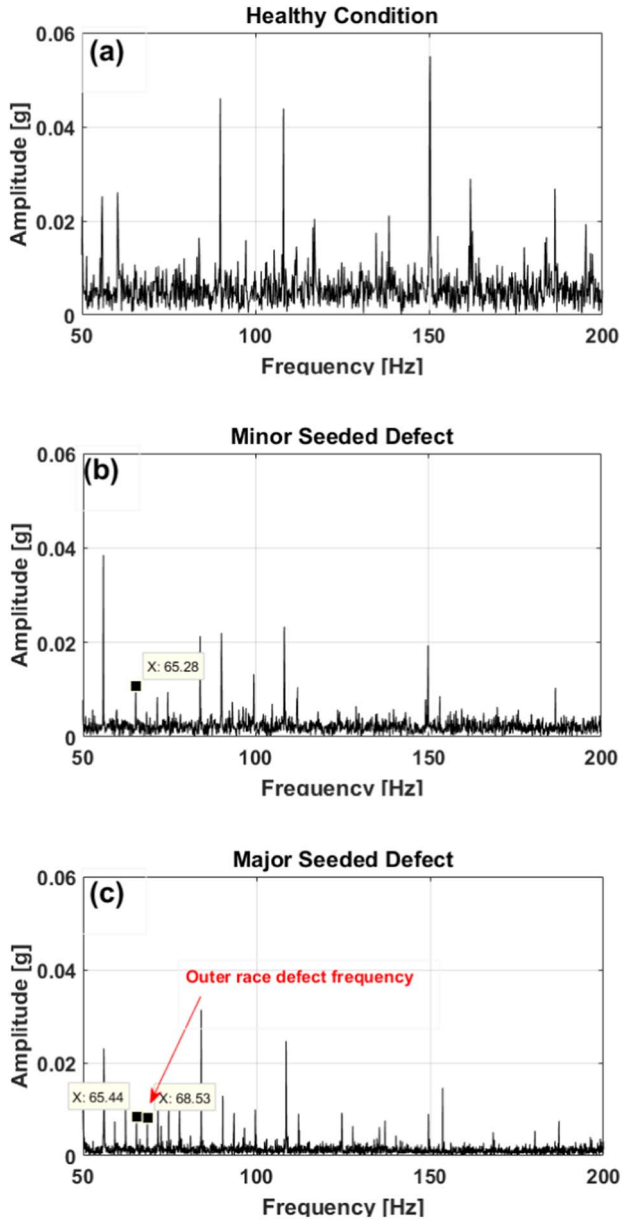

Fig. 12. Zoomed spectrum of raw data in test case 1, (a) healthy condition, (b) minor seeded defect condition and (c) major seeded defect condition.

2.3.2. Sensor selection and installation

To comply with the 500 g measuring range requirements, PCB 352C03 and Endevco 6251M4 sensors with 10 mv/g sensitivity were selected. Six accelerometers were chosen and bolted to the gearbox case. Since both input shafts were enabled, two accelerometers were attached at MGB case near input shaft. Two accelerometers were externally installed at the outer case of 2nd epicyclic ring gear. The other accelerometers were mounted at the MGB output modules RH and LH (Fig. 1).

2.3.3. Test procedures

Similar to test case 1, tests under three conditions were undertaken, including healthy condition, minor seeded defect condition and major seeded defect condition. Compared with test case 1, defects seeded in this test case were considerably larger. Fig. 9 demonstrates the major defect size, which was approximately 30 mm wide. This equals to 41° of the entire planetary bearing circumference. The minor defect size was chosen to be approximately 10 mm wide. The MGB was tested under various load conditions from 90 kW to 1760 kW, with input speed up to 23,000 rpm. All vibration data was recorded using NI 9234 data acquisition card with 51.2 kHz sampling frequency. This test case has been documented in detail in [19].

3. Planetary bearing defect diagnosis and signal processing

Vibration-based health monitoring (VHM) has been established as one of the key technologies implemented in HUMS. Many CIs and health indicators (HIs) were developed using vibration data to reflect the health state for gears, bearings and shafts in MGB [20]. However, as described in Section 1, HUMS is unable to provide reliable indications for planetary bearing defects. The reasons are manifold, including but not limited to:

- Sophisticated mechanical structures of multi-stage epicyclic reduction modules in MGB complicate the signal transmission paths [21]. Therefore, vibration data collected by accelerometers is severely modulated.
- Planetary bearings are encircled by planetary gears, which result in overwhelming gear mesh signals masking weak planetary bearing signals.
- High operational and background noise of helicopter MGB lowers the signal-to-noise (SNR) ratio, making it difficult to extract diagnostic information from collected data.
- Traditional condition indicators are generated based on statistical characteristics of vibration data, which sometimes demonstrate inconsistent trends. Interpretation of the corresponding indications is cumbersome.

To address these issues, signal processing techniques that excel at extracting hidden impulsive diagnostic information from noise and gear mesh signals should be investigated. Processing techniques including self-adaptive noise cancellation (SANC), kurtogram and envelope analysis are therefore employed in this study.

3.1. Self-adaptive noise cancellation

It is generally recognised that the vibration signal acquired from a complex mechanical system, which contains numerous shafts, gears and bearings, are overall stationary. This notion suggests that the mixed vibration signal have approximately constant statistical parameters, e.g. mean and standard deviation. The frequency spectrum of such signal is usually a mixture of discrete frequency components and continuous frequency components, which are excited by periodic gear meshes (deterministic) and random bearing signals with additive noise (non-deterministic), respectively [22,13,23]. Wold's theorem provides theoretical support to separate these two types of signal [24]. The theorem states that for any stationary process $X(n)$, the following representation exists:

$$X(n) = p(n) + r(n), \tag{1}$$

where $p(n)$ and $r(n)$ represent non-correlated deterministic process and non-deterministic zero mean process respectively. Signal $p(n)$ could be perfectly predicted from its past value, while $r(n)$ could not. Therefore, with an appropriate time delay chosen, non-deterministic bearing signals can no longer be predicted from its own delays, whereas deterministic gear signals can still be predicted. Based on this idea, Ho and Randall demonstrated the technique of separating non-deterministic bearing signals and discrete gear mesh signals using an adaptive filter in [8]. This technique is called self-adaptive noise cancellation (SANC) because it does not require reference noise signal as an extra input. In Fig. 10, the schematic diagram of SANC is depicted. The separation is achieved by adaptively filtering a delayed signal $X(n-\Delta)$ to predict original signal $X(n)$, generating prediction error $e(n)$. By selecting a proper delay Δ, the output from adaptive filter W will contain more

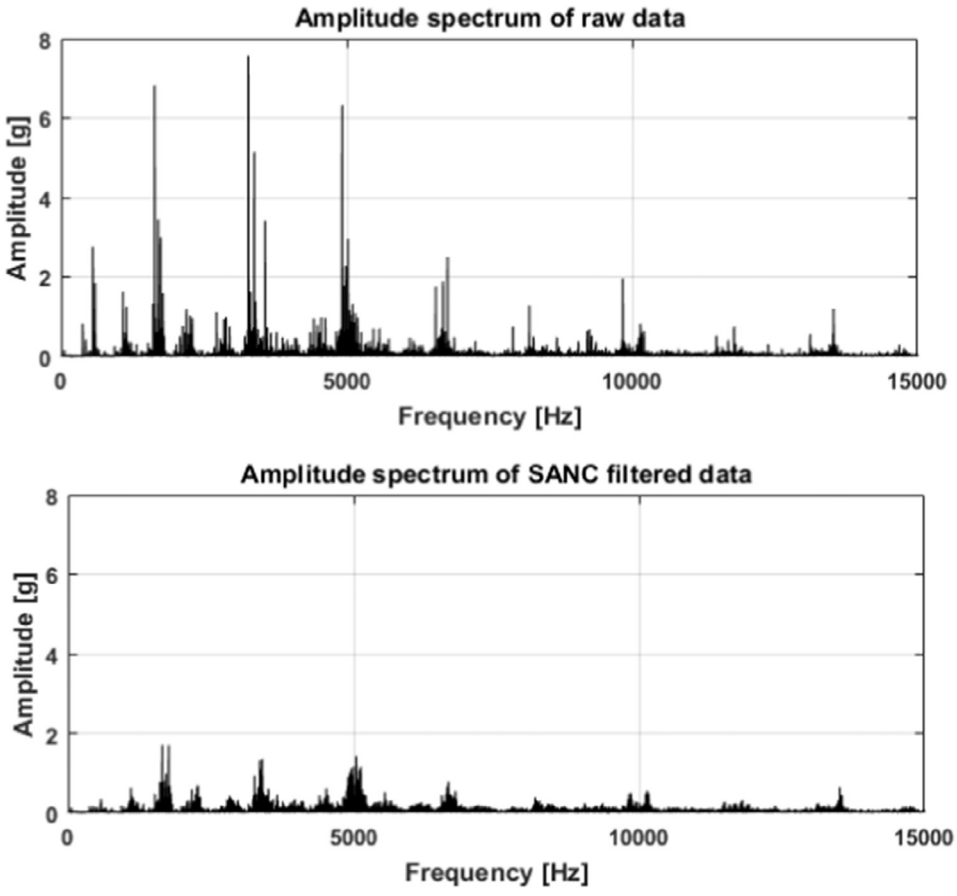

Fig. 13. SANC filter's effect of cancelling gear mesh frequencies.

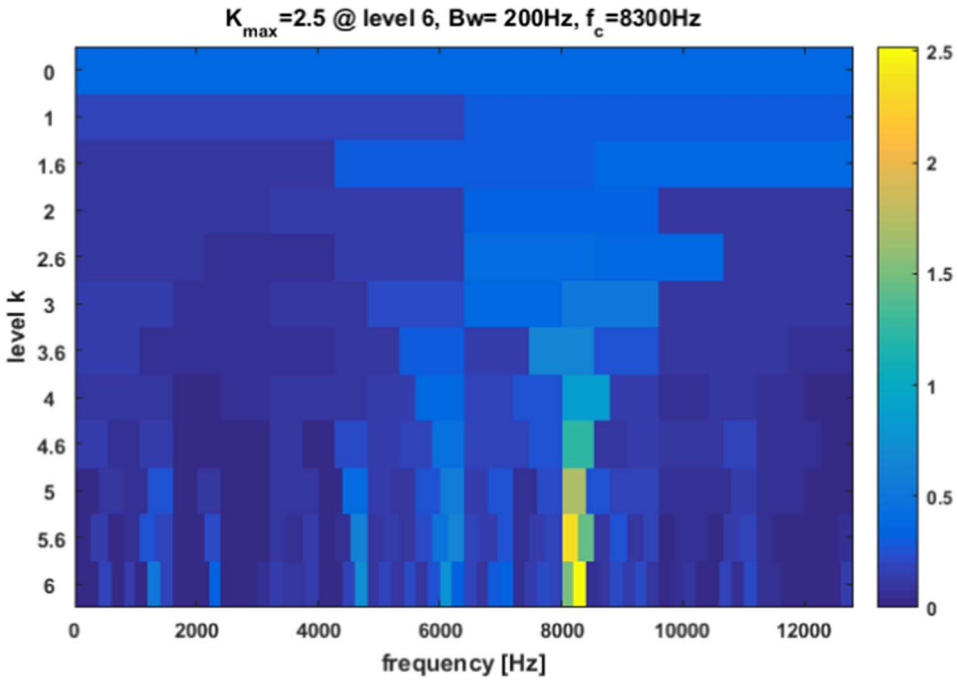

Fig. 14. Kurtogram indication of SANC filtered signal, minor seeded defect.

deterministic components, leaving the prediction error $e(n)$ contains mostly non-deterministic signals.

One of the most widely adopted adaptive filter is least mean square (LMS) filter. LMS filter's coefficients are adaptively updated until the mean square of prediction error $e(n)$ is minimised. LMS adaptation rule is defined as [8,25]:

$$e(n) = X(n) - W_n^T \cdot X(n-\Delta) \tag{2}$$

$$W_{n+1} = W_n + \mu \cdot e(n) \cdot X(n-\Delta), \tag{3}$$

where μ is the forgetting factor which determines the adaptation step, Δ is time delay, and W_{n+1} represents the filter coefficients in $n+1$ iteration. In [12], a very thorough guidance was given on how to choose the

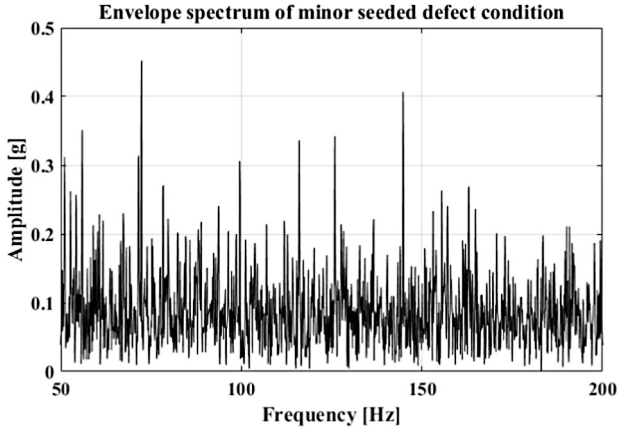

Fig. 15. Corresponding envelope spectrum of filtered signal, unsuccessful.

Table 6
Bandpass parameters for test case 1.

Test condition	Centre frequency [Hz]	Bandwidth [Hz]
Healthy	9793	200
Minor seeded defect	9802	250
Major seeded defect	9824	250

factor Δ and filter length. The selection of μ was discussed in classic articles [25,26]. The concept of SANC and its successful applications have been extensively discussed in [11,27–29].

3.2. Envelope analysis and kurtogram

Envelope analysis has been employed for bearing fault diagnosis for over 40 years [14]. It excels at revealing repetitive information hidden in signals' envelope, mitigating the effect of speed fluctuation, amplitude modulation, and additive noise [13]. Commonly, envelope analysis benefits considerably from band-passing vibration signal in a certain high frequency band, where the frequency resonances associated with planetary bearings are dominant [15]. The envelope of the bandpass signal is then obtained by performing Hilbert transform (HT). By examining the envelope spectrum of the band-passed signal, the diagnostic information of faulty bearing signals can be extracted for defect identification.

Successful implementation of envelope analysis requires one to have some knowledge of the suitable demodulating frequency band. In practice, this was used to be a mechanical problem. In [23], it is stated that there was a recommendation on using hammer tap testing to find out bearing housing resonances before the actual bearing tests, which was inconvenient. A mathematical tool, namely the kurtogram, was developed to solve this problem.

Kurtogram was developed from the concept of spectral kurtosis (SK), which was firstly devised by Dwyer in [30] for the detection of "randomly occurring signals " [31]. Antoni gave a detailed study of SK in [32,16], which demonstrated the potential applications of SK on bearing defect diagnosis. SK is defined as [23]:

$$SK(f) = \frac{E\{|X(t,f)|^4\}}{E\{|X(t,f)^2|\}^2} - 2, \tag{4}$$

where $E[\cdot]$ is the expectation operator. $E\{|X(t,f)|\}$ is considered as time average of the short-time Fourier transform (STFT) of the signal at time t, band-passed around frequency f. Therefore, SK evaluates the impulsiveness of the signal which is band-passed at different centre frequencies. Kurtogram demonstrates SK not only as function of t and f, but also as function of frequency bandwidth Δf, so that the values of SK calculated with different centre frequency and bandpass bandwidth can

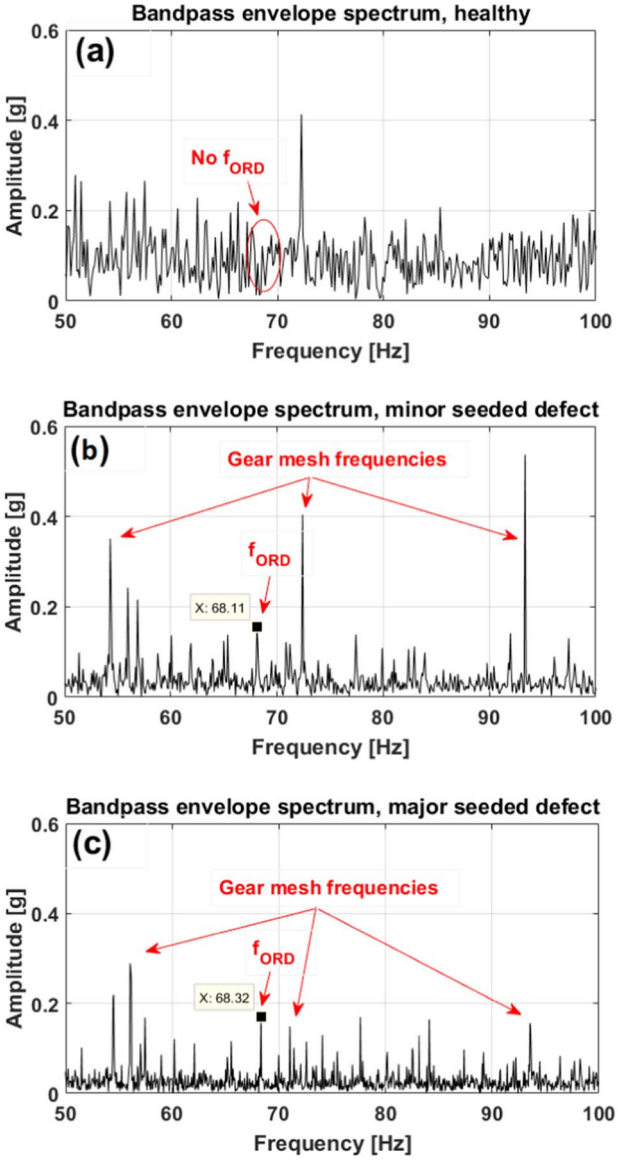

Fig. 16. Envelope spectrum of demodulated data in test case 1, (a) healthy condition, (b) minor seeded defect condition and (c) major seeded defect condition.

be portrayed in a colour map. Since kurtogram is able to provide indications on possible bandpass centre frequency as well as bandwidth, implementation of envelope analysis is much simplified. However, it is noted that the indication of kurtogram is not always correct, especially in our cases where multiple gear mesh frequencies and harmonics exist in the envelope spectrum. Under the circumstance where kurtogram fails to indicate accurately, suboptimal parameters of centre frequency and Δf for envelope demodulation are chosen by inspecting candidate resonances in frequency spectrum.

With the processing techniques introduced, the following processing procedures were implemented:

- Perform SANC to separate gear meshes and bearing-related signals.
- Perform kurtogram on separated bearing signals, selecting suitable centre frequency and frequency band for envelope demodulation.
- Perform envelope analysis to extract repetitive information in demodulated signal. The envelope spectrum will be examined for fault related frequency components.

The outer race defect frequency (f_{ORD}) is calculated using the equation below:

Table 7
Key frequency components of test case 2.

Speed of:	Frequency [Hz]
Input shaft	383.33
1st planetary carrier shaft	12.95
1st planetary gear meshes	1683.44
2nd planetary carrier shaft	4.44
2nd planetary gear meshes	578.15
Outer race defect frequency (f_{ORD}):	97.42

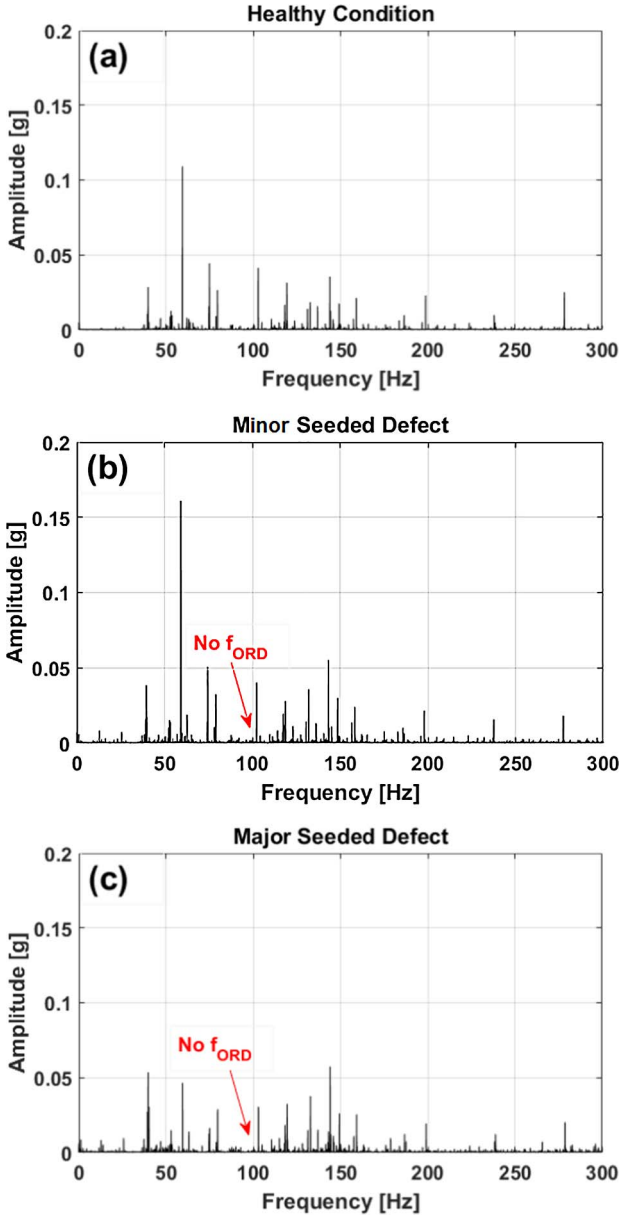

Fig. 17. Zoomed spectrum of raw data in test case 2, (a) healthy condition, (b) minor seeded defect condition and (c) major seeded defect condition.

$$f_{ORD} = \frac{N \cdot f_r}{2} \cdot \left(1 - \frac{d}{D} \cdot cos\phi\right), \tag{5}$$

where N is the number of rollers, f_r is shaft speed. d and D represent the roller's diameter and pitch diameter, respectively. ϕ is the contact angle between rollers and races. In practice, due to the slip of the rolling elements and the speed fluctuation, the extracted f_{ORD} usually presents several hertz offset from the calculated value.

4. Processing results

4.1. Processing results of test case 1

Vibration data collected under healthy, minor seeded defect and major seeded defect conditions was processed. The MGB was operated at 16,000 rpm input speed with 180 kW load. The data from triaxial accelerometer 1 in Fig. 5 was selected. This decision was made considering that accelerometer 1 has the shortest relative distance to the seeded defect, therefore defect signal was less attenuated during transmission. In addition, according to the report of G-REDL accident [33], using data from sensors which were not attached near 2nd epicyclic module may have contributed to the invalid diagnosis of 2nd planetary bearing defect in that accident. Hence data from accelerometer 1 was considered most relevant to identification of the seeded defect.

To assist the diagnosis in frequency domain, key frequency components are calculated and summarised in Table 5.

Fig. 11 shows the amplitude spectrum of vibration data under three conditions. It is observed that the spectrum are very similar to each other, where the discrete periodic gear meshes and their harmonics are dominant. Fig. 12 is produced by zooming Fig. 11 into frequency range of 50–200 Hz, for identification of possible f_{ORD} near 68 Hz. It is discovered in Fig. 12 that f_{ORD} cannot be found in healthy and minor seeded defect condition. In major seeded defect condition (Fig. 12(c)), the defect frequency of 68.53 Hz is evident. The marked 65.44 Hz frequency component is resulted from the 3.09 Hz modulation of 2nd planetary carrier.

In order to reveal distinct defect indications in minor and major seeded defect conditions, SANC was applied to process the data. Fig. 13 demonstrates the effect of applied SANC filter, where the large deterministic frequency components have been prominently eliminated. The filtered signal was further processed using kurtogram. The implemented kurtogram code was written in MATLAB by J. Antoni. Fig. 14 demonstrates the kurtogram of SANC filtered signal in minor seeded defect condition. Kurtogram indicates a candidate bandpass frequency at 8300 Hz with bandwidth of 200 Hz. However, this indication was discovered to be inaccurate. Fig. 15 shows the envelope spectrum of corresponding band-passed signal as suggested by the kurtogram result. No improvement of the signal-to-noise ratio was observed, compared with the result shown in Fig. 12(b). The same result was observed for data associated with the major seeded defect condition.

As the kurtogram analysis has failed to identify the optimal centre frequency and associated bandwidth for envelope analysis, the suboptimal parameters were determined by manually inspecting the envelope spectrum of other candidate frequency resonances in the amplitude spectrum of SANC filtered signal (Fig. 13). Bandpass parameters that offered optimal SNR improvements are recorded in Table 6.

Envelope analysis was performed on demodulated data. The envelope spectrum of healthy, minor fault and major fault condition are illustrated in Fig. 16.

It is shown in Fig. 16 that the bandpass envelope analysis has given decisive diagnosis results. The calculated f_{ORD} which is at 68 Hz can be identified in both minor and major fault conditions directly, while no f_{ORD} is indicated in healthy condition. It is also observed that in major seeded defect condition, the frequency sidebands around 68.32 Hz defect frequency are more intensely spread from 60 Hz to 90 Hz, compared with that shown in minor seeded defect condition. However, the amplitude of envelope spectrum cannot reflect the severity of the seeded defect based on the observations, such phenomenon has also been found in other papers using real data [34–36]. With defect frequency evidently extracted, diagnosis of planetary bearing outer race defect in Test case 1 is successful.

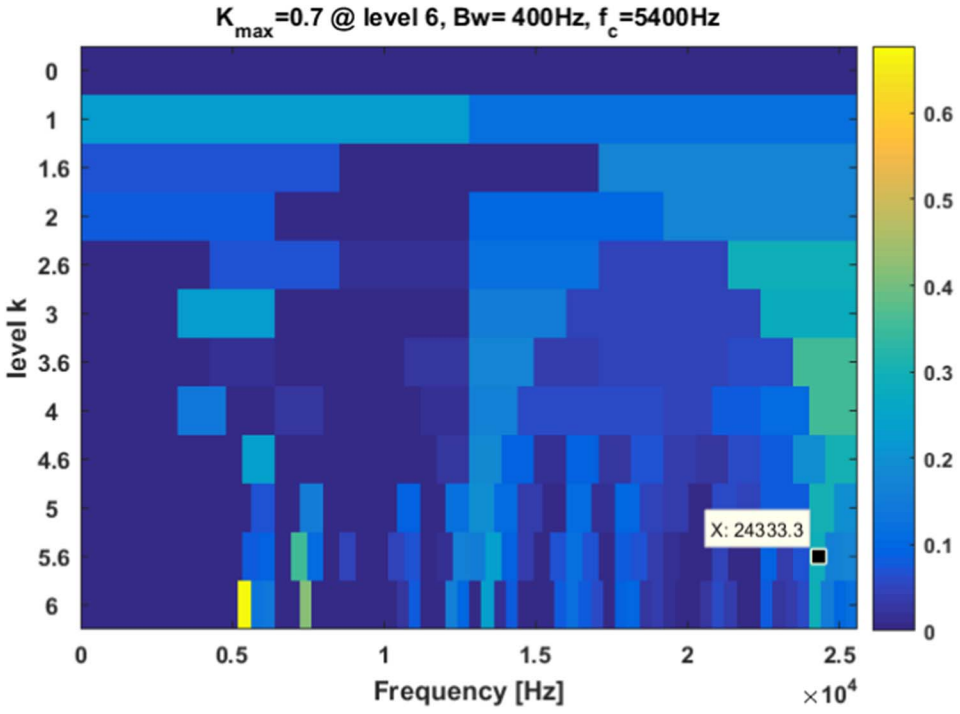

Fig. 18. Kurtogram of SANC filtered signal, minor seeded defect.

Table 8
Bandpass parameters for test case 2.

Test condition	Centre frequency [Hz]	Bandwidth [Hz]
Healthy	24,324	560
Minor seeded defect	24,316	560
Major seeded defect	24,354	600

4.2. Processing results of test case 2

In test case 2, MGB was operated at 23,000 rpm input speed with 1760 kW load. Key frequency components are calculated and summarised in Table 7.

Zoomed amplitude spectrum of raw vibration data is presented in Fig. 17. In all three conditions, discrete frequency components related to gear meshes are dominant across the zoomed frequency bandwidth. No direct indication of f_{ORD} can be identified at 97 Hz. It indicates that in this test case, very limited diagnostic information is revealed in lower range of the frequency spectrum, due to the severe operating conditions and distributed defects. In order to extract diagnostic information, SANC and kurtogram technique were implemented.

Fig. 18 shows kurtogram result of SANC filtered data in minor seeded defect condition. Kurtogram suggests that the suitable demodulation centre frequency was 5400 Hz with 400 Hz bandwidth. However, through exploring other centre frequencies, it was discovered that 24,333 Hz with approximately 600 Hz bandwidth were the optimal demodulation parameters. Similar inspections were conducted for major seeded defect conditions as well. The final bandpass parameters for three conditions are determined, and listed in Table 8.

Envelope analysis was then implemented using parameters in Table 8. The envelope spectrum of demodulated data in healthy, minor seeded defect condition and major seeded defect condition are shown in Fig. 19. It is evident that the fault related frequency component f_{ORD} (near 97 Hz) along with its harmonics are distinct for both minor and major seeded defect conditions. In the meantime, the sidebands labelled near 93 Hz and 101 Hz in both the faulty conditions can also be identified. These sidebands are resulted from 4.4 Hz 2nd planetary carrier speed modulation. This indicates an indisputable success in diagnosing planetary bearing outer race defect.

5. Discussion and conclusion

In this paper, MGB planetary bearing outer race defect diagnosis is investigated. To support this study, special test rigs were designed with commercial helicopter main gearbox SA330. Vibration data under healthy, minor seeded defect condition and major seeded defect condition were recorded in two test cases, where MGB was operated at 16,000 rpm with 180 kW load and at 23,000 rpm with 1760 kW load respectively. Signal processing techniques including SANC, kurtogram and envelope analysis were employed to extract fault-related bearing signals which were originally masked.

SANC was applied to separate periodic gear mesh signals and random bearing signals using adaptive filter. Kurtogram was applied to reveal hidden impulsive signatures which were associated with bearing defect in high frequency bands. Envelope analysis was performed to extract repetitive signals which were excited by bearing defect. However, processing results in Figs. 14 and 18 show that kurtogram cannot always generate accurate indications of the most impulsive frequency component for MGB vibration data. This is because that transmission paths for MGB vibration data are continuously varying due to the rotation of 1st and 2nd epicyclic module. Moreover, planetary gear meshes cannot be completely eliminated by adaptive filtering, making kurtogram insensitive to hidden impulsive bearing signals. Tian et al. [37] also described and analysed the deficiency of kurtogram in detecting the non-deterministic signals masked by strong noise in planetary system. Overall, the diagnosis in both 16,000 rpm test case and 23,000 rpm test case are successful. The calculated outer race defect frequency f_{ORD} has been evidently identified in the envelope spectrum of the demodulated signals under all faulty conditions. Signal processing with aforementioned techniques has achieved indisputable success, specifically in test case 2 (Fig. 19), indicating that vibration data recorded in test case 2 contains more diagnostic bearing information than data recorded in test case 1.

In this study, the extraction of diagnostic information is presented, which facilitates accurate and sensitive CIs to be designed, hence enhancing the capabilities of HUMS to detect MGB planetary bearing defects.

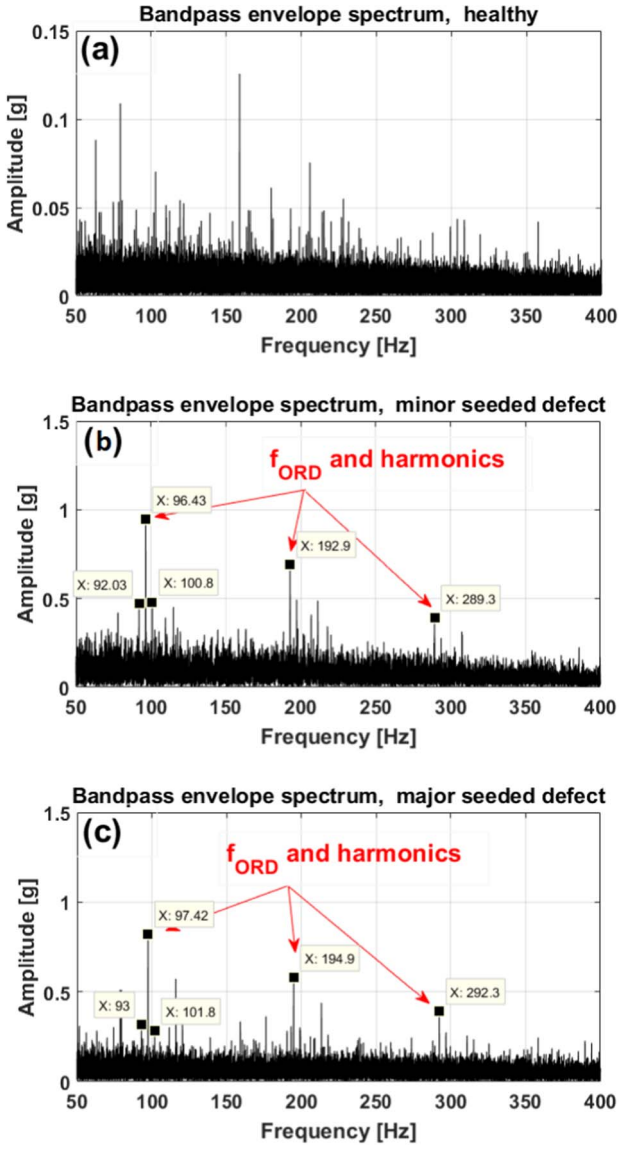

Fig. 19. Envelope spectrum of demodulated data in test case 2, (a) healthy condition, (b) minor seeded defect condition and (c) major seeded defect condition.

Acknowledgement

This study is sponsored by European Aviation Safety Agency (EASA), project entitled “MGH - Helicopter main gearbox health”.

References

[1] Land JE. Hums-the benefits-past, present and future. IEEE proceedings aerospace conference, 2001, vol. 6. IEEE; 2001. p. 3083–94.
[2] Joint Helicopter Safety Implementation Team. Health and usage monitoring systems toolkit.
[3] IHST. Worldwide accident rate. < http://www.ihst.org/Default.aspx?tabid=3056&language=en-US > .
[4] Pipe K. Measuring the performance of a hum system-the features that count. In: Third international conference on health and usage monitoring-HUMS2003; 2002. p. 5.
[5] Air Accidents Investigation Branch. Report on the accident to Aerospatiale Eurocopter AS332 L2 super puma, registration G-REDL 11 nm NE of Peterhead, Scotland on 1 April 2009. Tech rep. Air Accidents Investigation Branch; 2009.
[6] AAIB. AAIB special bulletin to EC225 LP super puma, G-REDW accident. Tech rep. Air Accidents Investigation Branch; 2016.
[7] AIBN. Accident at Turoy, near Bergen, Norway on 29 April 2016, involving Airbus helicopters H225, LN-OJF. Tech rep. Accident Investigation Board Norway; 2016.
[8] Ho D, Randall R. Effects of time delay, order of fir filter and convergence factor on self-adaptive noise cancellation. In: International Conference on Sound and Vibration (ICSV5), Adelaide; 1997.
[9] Ho D, Randall R. Optimisation of bearing diagnostic techniques using simulated and actual bearing fault signals. Mech Syst Signal Process 2000;14(5):763–88.
[10] Ruiz-Carcel C, Hernani-Ros E, Chandra P, Cao Y, Mba D. Application of linear prediction, self-adaptive noise cancellation, and spectral kurtosis in identifying natural damage of rolling element bearing in a gearbox. Proceedings of the 7th World Congress on Engineering Asset Management (WCEAM 2012). Springer; 2015. p. 505–13.
[11] Bonnardot F, Randall RB, Antoni J, Guillet F. Enhanced unsupervised noise cancellation (e-sanc) using angular resampling application for planetary bearing fault diagnosis. Surveillance 2004;5:11–3.
[12] Antoni J, Randall R. Unsupervised noise cancellation for vibration signals: Part i – Evaluation of adaptive algorithms. Mech Syst Signal Process 2004;18(1):89–101.
[13] Randall RB. Vibration-based condition monitoring: industrial, aerospace and automotive applications. John Wiley & Sons; 2011.
[14] Darlow MS, Badgley RH, Hogg G. Application of high-frequency resonance techniques for bearing diagnostics in helicopter gearboxes. Tech rep; 1974.
[15] McFadden P, Smith J. Vibration monitoring of rolling element bearings by the high-frequency resonance technique – a review. Tribol Int 1984;17(1):3–10.
[16] Antoni J, Randall R. The spectral kurtosis: application to the vibratory surveillance and diagnostics of rotating machines. Mech Syst Signal Process 2006;20(2):308–31.
[17] Delgado IR, Dempsey PJ, Simon DL. A survey of current rotorcraft propulsion health monitoring technologies; 2012.
[18] U.S.A. Aviation, M. Command. Aeronautical design standard handbook for condition based maintenance systems for US army aircraft systems. Tech rep.
[19] Greaves M, Elasha F, Worskett J, Mba D, Rashid H, Keong R. Vhm: vibration health or alternative monitoring technologies for helicopters. Tech rep. European Aviation Safety Agency; 2012.
[20] A. Aviation, M.L.C. Command. Ads-79b-hdbk (2011), handbook for condition based maintenance systems for us army aircrafts; 2011.
[21] Fraser K. An overview of health and usage monitoring systems (hums) for military helicopters. Tech rep; 1994.
[22] Antoni J, Randall R. Differential diagnosis of gear and bearing faults. Trans-Am Soc Mech Eng J Vib Acoust 2002;124(2):165–71.
[23] Randall RB, Antoni J. Rolling element bearing diagnostics – a tutorial. Mech Syst Signal Process 2011;25(2):485–520.
[24] Wold H. A study in the analysis of stationary time series; 1939.
[25] Widrow B, Glover JR, McCool JM, Kaunitz J, Williams CS, Hearn RH, et al. Adaptive noise cancelling: principles and applications. Proc IEEE 1975;63(12):1692–716.
[26] Haykin SS. Adaptive filter theory. Pearson Education India; 2008.
[27] Elasha F, Ruiz-Carcel C, Mba D, Chandra P. A comparative study of the effectiveness of adaptive filter algorithms, spectral kurtosis and linear prediction in detection of a naturally degraded bearing in a gearbox. J Fail Anal Prevent 2014;14(5):623–36.
[28] Barszcz T. Decomposition of vibration signals into deterministic and non-deterministic components and its capabilities of fault detection and identification. Int J Appl Math Comput Sci 2009;19(2):327–35.
[29] Randall R, Sawalhi N, Coats M. A comparison of methods for separation of deterministic and random signals. Int J Cond Monitor 2011;1(1):11–9.
[30] Dwyer R. Use of the kurtosis statistic in the frequency domain as an aid in detecting random signals. IEEE J Ocean Eng 1984;9(2):85–92.
[31] Vrabie V, Granjon P, Serviere C. Spectral kurtosis: from definition to application. In: 6th IEEE international workshop on Nonlinear Signal and Image Processing (NSIP 2003); 2003.
[32] Antoni J. The spectral kurtosis: a useful tool for characterising non-stationary signals. Mech Syst Signal Process 2006;20(2):282–307.
[33] Jarvis MP, Sleight P. Report on the accident to aerospatiale (Eurocopter) AS332 L2 super puma registration G-REDL. Aircraft Accid Rep 2011;2(2011):24.
[34] Feng Z, Zuo MJ. Vibration signal models for fault diagnosis of planetary gearboxes. J Sound Vib 2012;331(22):4919–39.
[35] Liu J, Wang W, Golnaraghi F, Liu K. Wavelet spectrum analysis for bearing fault diagnostics. Meas Sci Technol 2007;19(1):015105.
[36] Zhang M, Jiang Z, Feng K. Research on variational mode decomposition in rolling bearings fault diagnosis of the multistage centrifugal pump. Mech Syst Signal Process 2017;93:460–93.
[37] Tian X, Gu JX, Rehab I, Abdalla GM, Gu F, Ball AD. A robust detector for rolling element bearing condition monitoring based on the modulation signal bispectrum and its performance evaluation against the kurtogram. Mech Syst Signal Process 2018;100:167–87.